Clim Dyn (2015) 44:2447–2462
DOI 10.1007/s00382-014-2379-y

Tropical Indian Ocean subsurface temperature variability and the forcing mechanisms

Ojha Sayantani · C. Gnanaseelan

Received: 27 December 2013 / Accepted: 14 October 2014 / Published online: 21 October 2014

Abstract The first two leading modes of interannual variability of sea surface temperature in the Tropical Indian Ocean (TIO) are governed by El Niño Southern Oscillation and Indian Ocean Dipole (IOD) respectively. TIO subsurface however does not co-vary with the surface. The patterns of the first mode of TIO subsurface temperature variability and their vertical structure are found to closely resemble the patterns of IOD and El Niño co-occurrence years. These co-occurrence years are characterized by a north–south subsurface dipole rather than a conventional IOD forced east–west dipole. This subsurface dipole is forced by wind stress curl anomalies, driven mainly by meridional shear in the zonal wind anomalies. A new subsurface dipole index (SDI) has been defined in this study to quantify the intensity of the north–south dipole mode. The SDI peaks during December to February (DJF), a season after the dipole mode index peaks. It is found that this subsurface north–south dipole is a manifestation of the internal mode of variability of the Indian Ocean forced by IOD but modulated by Pacific forcing. The seasonal evolution of thermocline, subsurface temperature and the corresponding leading modes of variability further support this hypothesis. Positive wind stress curl anomalies in the south and negative wind stress curl anomalies in the north of 5°S force (or intensify) downwelling and upwelling waves respectively during DJF. These waves induce strong subsurface warming in the south and cooling in the north (especially during DJF) and assist the formation and/or maintenance of the north–south subsurface dipole. A thick barrier layer forms in the southern TIO, supporting the long persistence of anomalous subsurface warming. To the best of our knowledge the existence of such north–south subsurface dipole in TIO is being reported for the first time.

Keywords Indian Ocean · Subsurface variability · IOD · El Nino · Interannual variability

1 Introduction

El Niño Southern Oscillation (ENSO), believed to be the strongest climate modulator in the tropics on interannual time scale is a clear example emphasizing the influence of subsurface ocean on Sea Surface Temperature (SST) and the atmosphere (Bjerknes 1969; Neelin et al. 1998). ENSO effects are bridged ("atmospheric bridge", Nigam and Shen 1993; Klein et al. 1999; Lau and Nath 2000) to the Tropical Indian Ocean (TIO) primarily by the zonal displacement of the convergence centers associated with Walker circulation. This induces subsidence in the eastern TIO resulting in suppressed rainfall and anomalous easterly winds (Lau and Nath 2000; Shinoda et al. 2004) followed by a basin wide TIO warming due to increase in the short wave radiation and decrease in the latent heat flux (Yu and Reinecker 1999; Chowdary and Gnanaseelan 2007). This warming is the dominant mode of interannual variability in TIO SST. As the mean thermocline in the TIO is deep compared to the east Pacific it was believed for a long time that the TIO merely responds to Pacific forcing in the interannual time scale. However Saji et al. (1999) and Webster et al. (1999) showed that TIO can develop its own internal mode of SST variability (Indian Ocean Dipole, IOD) through coupled ocean–atmosphere processes. The typical IOD manifests itself through a zonal gradient of tropical SST anomalies with cooling off Sumatra and warming in the western TIO (Saji et al. 1999; Webster et al. 1999; Murtugudde et al.

O. Sayantani · C. Gnanaseelan (✉)
Indian Institute of Tropical Meteorology, Pune 411008, India
e-mail: seelan@tropmet.res.in

2000; Saji and Yamagata 2003). As the IOD develops, an east–west dipole of anomalous rainfall is also established over the TIO during September to November (SON), resulting in increased precipitation in the west and suppressed precipitation in the east (Saji et al. 1999; Webster et al. 1999). It is important to note that about half of the IOD co-occurred with El Niño (hereafter referred as co-occurrence years) and the remaining events developed internally in the TIO (Meyers et al. 2007) in the recent years. IOD usually is initiated in June-July and peaks in September or October (Saji et al. 1999) and are characterized by equatorial easterlies and upwelling along the coast of Sumatra. In the years of co-occurrence, ENSO variability is found to affect the periodicity, strength, and formation processes of the IOD (Annamalai et al. 2003; Behera et al. 2006). During the co-occurrence years IOD is stronger and persistent and are characterized by both the eastern cooling and western warming.

Dominant modes of interannual variability in the TIO surface and subsurface temperature do not show co-variability unlike in the Pacific Ocean (Rao et al. 2002). In the Pacific Ocean the subsurface temperature variability plays an important role in the evolution of SST associated with ENSO. In the TIO the first mode of SST variability shows a basin wide warming associated with ENSO mainly through the atmospheric bridge (Klein et al. 1999; Alexander et al. 2002; Yang et al. 2007; Chowdary and Gnanaseelan 2007). But the dominant subsurface mode of variability reported by Rao et al. (2002) is an east–west dipole forced by IOD. However, their conclusion is based on the composite consisting of both pure IOD and co-occurrence events and so it is important to examine the pattern of variability during the co-occurrence years. Using Ocean General Circulation Model experiments, Shinoda et al. (2004) found that ENSO induced surface zonal wind anomalies can sometime trigger a dynamically controlled subsurface dipole in the TIO. Rao and Behera (2005) discussed the role of subsurface on SST variability for both northern and southern TIO. Two distinguished regions of subsurface influence on SST are identified. Yu et al. (2005) and Rao and Behera (2005) showed that IOD dominates the forcing in the region north of 10°S and El Niño dominates the forcing south of 10°S. On the other hand Xie et al. (2002) observed anomalous downwelling Rossby waves along 10°S during El Niño years. Positive SST anomalies over this region are found to co-propagate with this Rossby wave, strongly indicating a subsurface-surface feedback (Xie et al. 2002; Huang and Kinter 2002; Chowdary et al. 2009). The relative effect of El Niño and IOD in generating downwelling Rossby waves over this region is discussed by Yu et al. (2005), Rao and Behera (2005), Chowdary and Gnanaseelan (2007), Gnanaseelan et al. (2008), Gnanaseelan and Vaid (2010) and Chakravorty et al. (2014). All the previous studies on the subsurface variability are based on either pure IOD years or on the combination of pure IOD and co-occurrence years and did not separately account for the IOD events that co-occur with El Niño. We have studied the TIO subsurface variability in pure IOD, pure El Niño and co-occurrence composites to better understand the forcing mechanism and subsurface response. The subsurface warming in all the cases and the associated processes are also discussed in detail. The mechanism for the long persistence of warming and the associated air–sea interaction are also studied. The paper further examines the vertical structure of subsurface warming in the southern TIO, its westward propagation and the associated mechanisms during the pure IOD, pure El Niño and co-occurrence years.

2 Data and methodology

Simple Ocean Data Assimilation (SODA) version 2.1.6 monthly product (Carton and Giese 2008) for the 50 years period of January 1958 to December 2007 is used in the present study. SODA is an ocean model product based on Parallel Ocean Program (POP) physics. SODA assimilates temperature and salinity profiles from the World Ocean Atlas (MBT, XBT, CTD, and station data), as well as additional hydrography, SST, and altimeter sea surface height (SSH) anomalies. The model is forced with the 40-year European Centre for Medium-Range Weather Forecasts (ECMWF) Reanalysis (ERA-40) (Uppala et al. 2005) daily atmospheric winds (Simmons and Gibson 2000) for the 44 years period from 1958 to 2001 and subsequently with Quikscat winds from 2002 onwards. SODA temperature, salinity and SSH data are extensively used in the analysis. The depth of 20 °C isotherm (d20) is computed from SODA temperature field. Surface winds and total column water vapor data from ERA-40 during 1958–2001 and ERA-Interim during 2002–2007 are also used for the analysis. The empirical orthogonal function (EOF) of d20 and 100 m temperature anomalies are computed for the entire time series and for three different seasons (fall, winter and spring). For the seasonal EOF analysis the data for the respective seasons only are considered instead of the entire time series.

Isothermal layer depth (ILD) is calculated using SODA temperature. Mixed layer depth (MLD), and barrier layer thickness (BLT) are calculated using SODA temperature and salinity. The ILD is defined as the depth at which temperature falls by 0.8 °C from the surface temperature as in Kara et al. (2000). The definition of MLD is based on a variable potential density (σ_θ) criterion (Lukas and Lindstrom 1991; Sprintall and Tomczak 1992), which determines the depth at which σ_θ exceeds the surface value by the amount corresponding to the 0.8 °C decrease in temperature as in

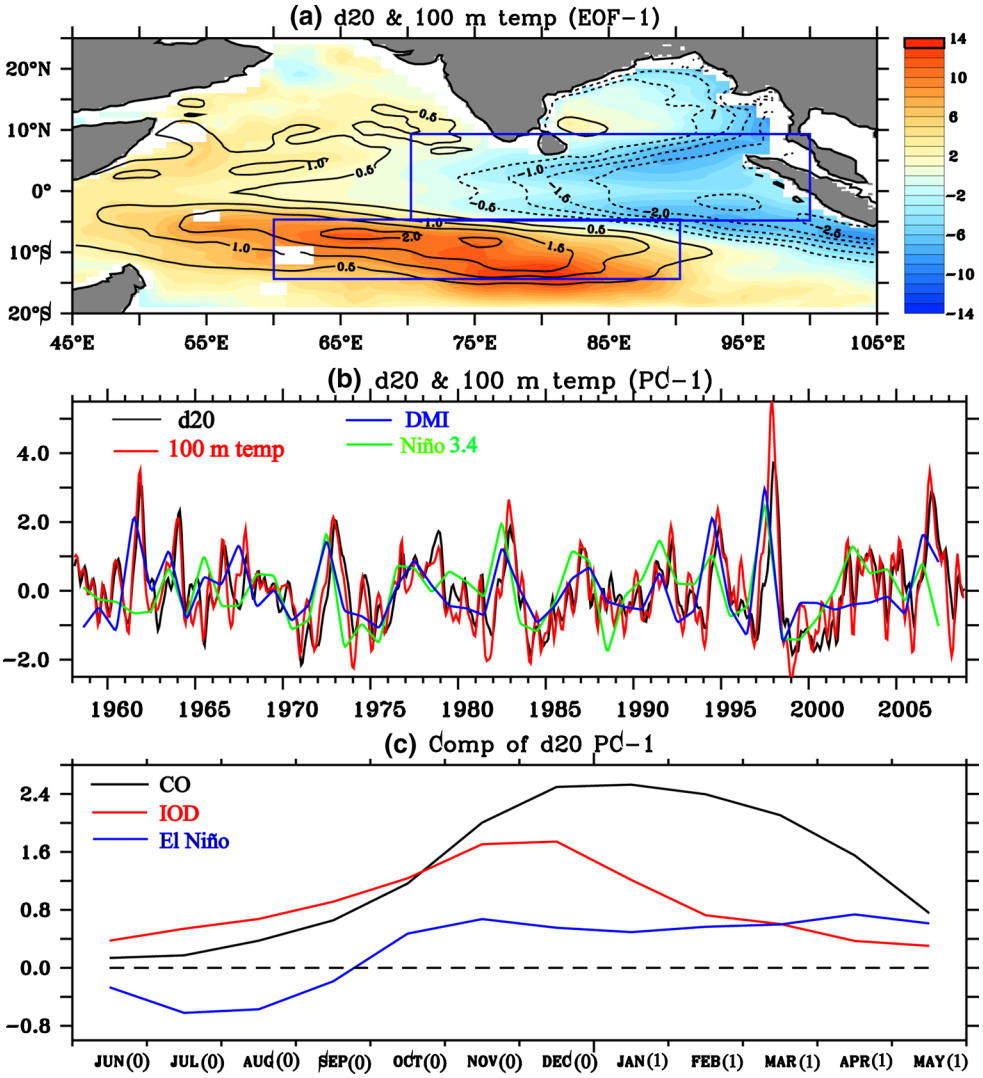

Fig. 1 **a** EOF1 of d20 anomalies (*shaded*, m) and 100 m temperature (*contours*, °C), **b** PC1 of d20 anomalies (*black*, m) and 100 m temperature (*red*, °C), and time series of DMI (*blue*, SON) and Niño 3.4 index (*green*, NDJ), **c** composite of PC1 of d20 anomalies (m) for co-occurrence (*black*), pure IOD (*red*) and pure El Niño (*blue*) years

Sayantani et al. (2013). BLT is computed as the difference between ILD and MLD. Composite analysis of pure IOD (1961, 1967, 1977, and 1994), co-occurrence (1963, 1972, 1982, 1997, and 2006) and pure El Niño (1965, 1976, 1986–1987, 2002) years is carried out to understand the interannual variability and its associated mechanism during 1958–2007. The list of years selected for the composites is based on Meyers et al. (2007) and Gnanaseelan et al. (2012).

3 Results and discussion

EOF analysis is carried out to identify the dominant modes of variability in d20 and 100 m temperature anomalies of TIO. The spatial pattern of the dominant mode of variability displays a strong north–south dipole instead of a conventional east–west dipole reported in literature (Fig. 1). It is important to note that though the first principal component (PC1) peaks in both pure IOD and co-occurrence years, the peak in the co-occurrence composite persists for more than two seasons with significantly higher amplitude unlike in pure IOD composite, where the peak is apparent only during SON. PC1 of d20 and 100 m temperature anomalies show significant correlation with both dipole mode index (DMI) and Niño 3.4 index (0.8 and 0.7 respectively). This suggests a possible role of El Niño in TIO subsurface temperature variability. To explore this further we examined the subsurface variability during different seasons [SON, December to February (DJF) and March to May (MAM)] separately. Subsurface temperature anomalies of SON display both north–south and east–west dipoles (Fig. 2a). Whereas, they are characterized by north–south dipole during DJF and MAM (Fig. 2b, c). Though IOD forcing weakens after November the subsurface anomalies persist during DJF (Fig. 2b) and MAM (Fig. 2c). The variability during SON is strongly associated with IOD but the possible role of El Niño is apparent during DJF as the leading mode

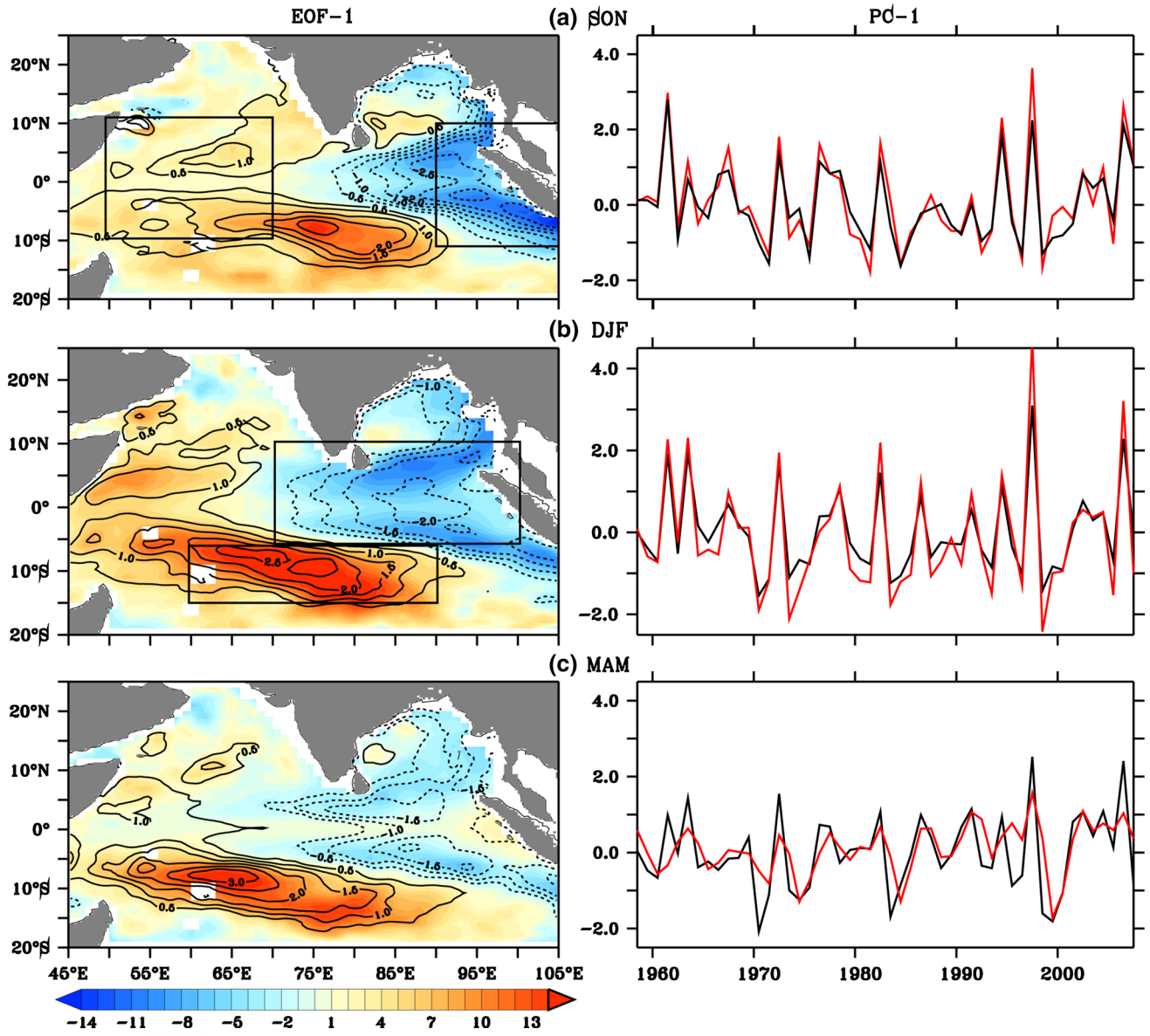

Fig. 2 EOF1 of d20 anomalies (*shaded*, m) and 100 m temperature (*contours*, °C) and PC1 of d20 anomalies (*black*, m) and 100 m temperature (*red*, °C) for **a** September–November, **b** December–February and **c** March–May

corresponds to the pattern of co-occurrence events. So we speculate that the subsurface variability and its north–south dipole pattern could be internally generated by IOD forcing but modulated by El Niño forcing.

Figure 3 displays the seasonal (SON, DJF, and MAM) composite of d20 and 100 m temperature anomalies during co-occurrence, pure IOD and pure El Niño years. The dominant north–south dipole is apparent in the co-occurrence composite whereas east–west dipole is evident in the pure IOD composite. It is interesting to note that the variability persists up to MAM in both d20 and 100 m temperature anomalies during the co-occurrence years. The spatial pattern of seasonal composites of d20 and 100 m temperature anomaly in the co-occurrence years (Fig. 3) are similar to the respective leading EOFs (Fig. 2). In co-occurrence years the north–south dipole is apparent in SON which strengthens in DJF. On the other hand the pure IOD composite shows a dominant east–west dipole pattern. In pure El Niño years the d20 anomaly is weak in SON but it strengthens in the following seasons. We have defined an index to quantify the strength of the north–south dipole in the subsurface temperature (and d20) and referred to as subsurface dipole index (SDI). It is computed as the difference in d20 anomalies between the regions 60°E–90°E, 15°S–5°S and 70°E–100°E, 5°S–10°N. The time series of DJF SDI is shown in Fig. 4a. The significant subsurface

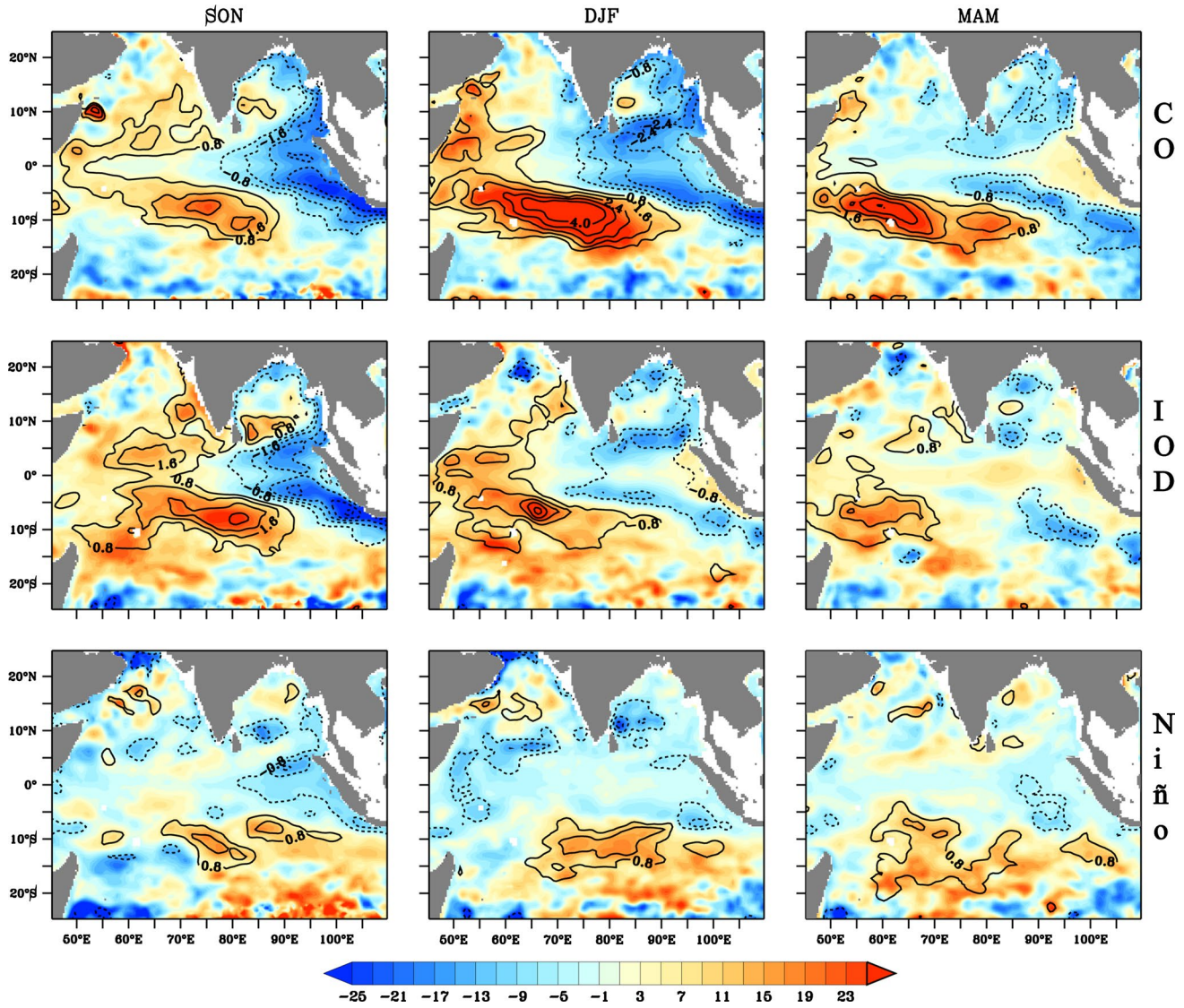

Fig. 3 Composite of anomalous d20 (*shaded*, m) and 100 m temperature (*contours*, °C) for co-occurrence (*upper panel*), pure IOD (*middle panel*) and pure El Niño (*bottom panel*) years

dipole events coincide mainly with the co-occurrence years though there are years when subsurface dipole events coincide with pure IOD (1961) or pure El Niño (1986–1987). We found that the correlation between SDI and DMI is 0.8, while between SDI and Niño 3.4 index is 0.7. We carried out partial correlation analysis to cleanly separate out the IOD and El Niño forcing responsible for the north–south dipole. The partial correlation between SDI and DMI is found to be 0.49, whereas between SDI and Niño 3.4 index is found to be 0.45. This suggests that IOD remains as a dominant forcing during co-occurrence years. SDI (Fig. 4b) peaks in January (1) with significant positive values up to April (1) in co-occurrence composite whereas the corresponding DMI peaks in November (0) ('0' represents El Niño developing year and '1' represents the decaying year). In pure IOD years SDI peaks in November (0) whereas DMI peaks in October (0). SDI shows relatively weaker amplitude in pure El Niño years but is positive up to April (1).

Anomalous equatorial easterlies during IOD and El Niño years induce anomalous anticyclonic wind stress curl on both sides of the equator and are favorable for equatorial and off-equatorial waves (Xie et al. 2002). The easterlies induce upwelling along the equator which then propagates eastward as equatorial upwelling Kelvin waves (Rao et al. 2010; Sreenivas et al. 2012). These waves after hitting the east coast propagate poleward as coastal Kelvin waves. Part of the energy is reflected from the coast as upwelling Rossby waves (Shinoda et al. 2004). On the other hand the anticyclonic wind stress curl induces off-equatorial

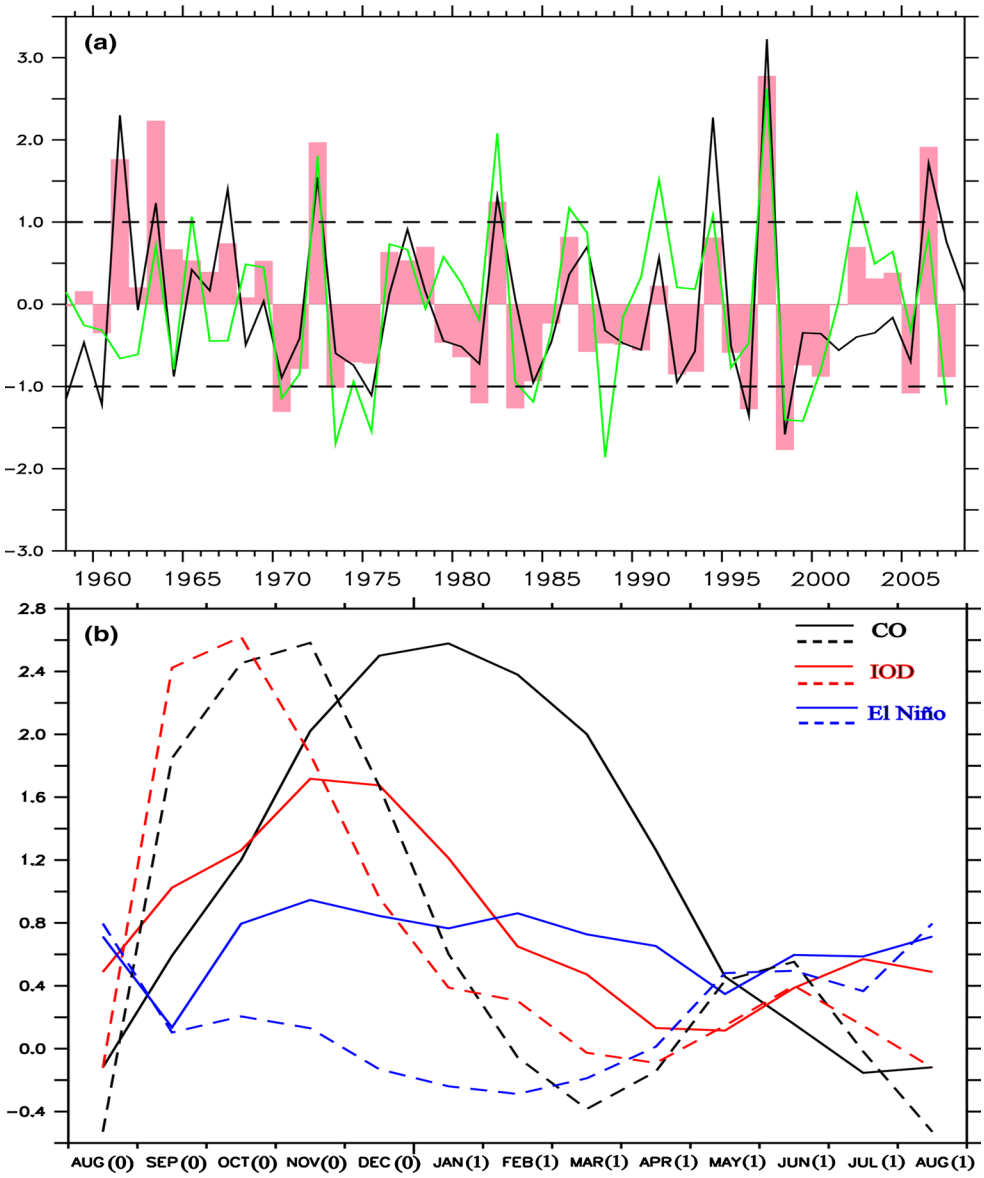

Fig. 4 *Bar* diagram of DJF SDI and DMI (*black line*) and Niño 3.4 index (*green line*) (*upper panel*). Composite of SDI (*solid line*) and DMI (*dashed line*) for co-occurrence (*black*), pure IOD (*red*) and pure El Niño (*blue*) years (*lower panel*)

downwelling Rossby waves on both north and south of the equator (Chambers et al. 1999; Gnanaseelan and Vaid 2010). It is important to note that the easterly wind anomalies have a much broader meridional scale south of equator than north during the co-occurrence years especially from December onwards (Fig. 5a). The zonal wind shear is maximum in November (0) during both pure IOD and co-occurrence years (Fig. 5b, c). However, it persists up to February (1) in co-occurrence years in the southern TIO.

It is evident from Fig. 5a that anomalous easterlies are mostly centered at equator during SON in both pure IOD and co-occurrence composites. Easterly wind maximum is shifted to 5°S during DJF in co-occurrence years (Fig. 5a). SST warming along the Rossby wave path enhances precipitation (Xie et al. 2002) and the associated convection intensifies easterlies over the region centered at 5°S during the co-occurrence years (Fig. 5a). These intensified easterlies induce meridional shear in zonal wind anomalies. These zonal wind shear anomalies induce positive wind stress curl anomaly in the south and negative wind stress curl anomaly in the north of 5°S (Fig. 6a, b) in co-occurrence years during DJF. The downwelling favorable shear in the southern TIO and the associated anti-cyclonic circulation support subsurface warming. Enhanced air–sea interaction and the associated wind stress curl anomalies induced by meridional shear in the zonal wind anomalies play an important role in the slow westward propagation of anomalous subsurface warming. It is important to note that there is no meridional asymmetry in the wind stress curl in pure IOD years (Fig. 6c, d) especially during DJF. The wind stress curl shows weak anomaly during SON in pure El Niño years but strengthens during DJF (Fig. 6e, f). In

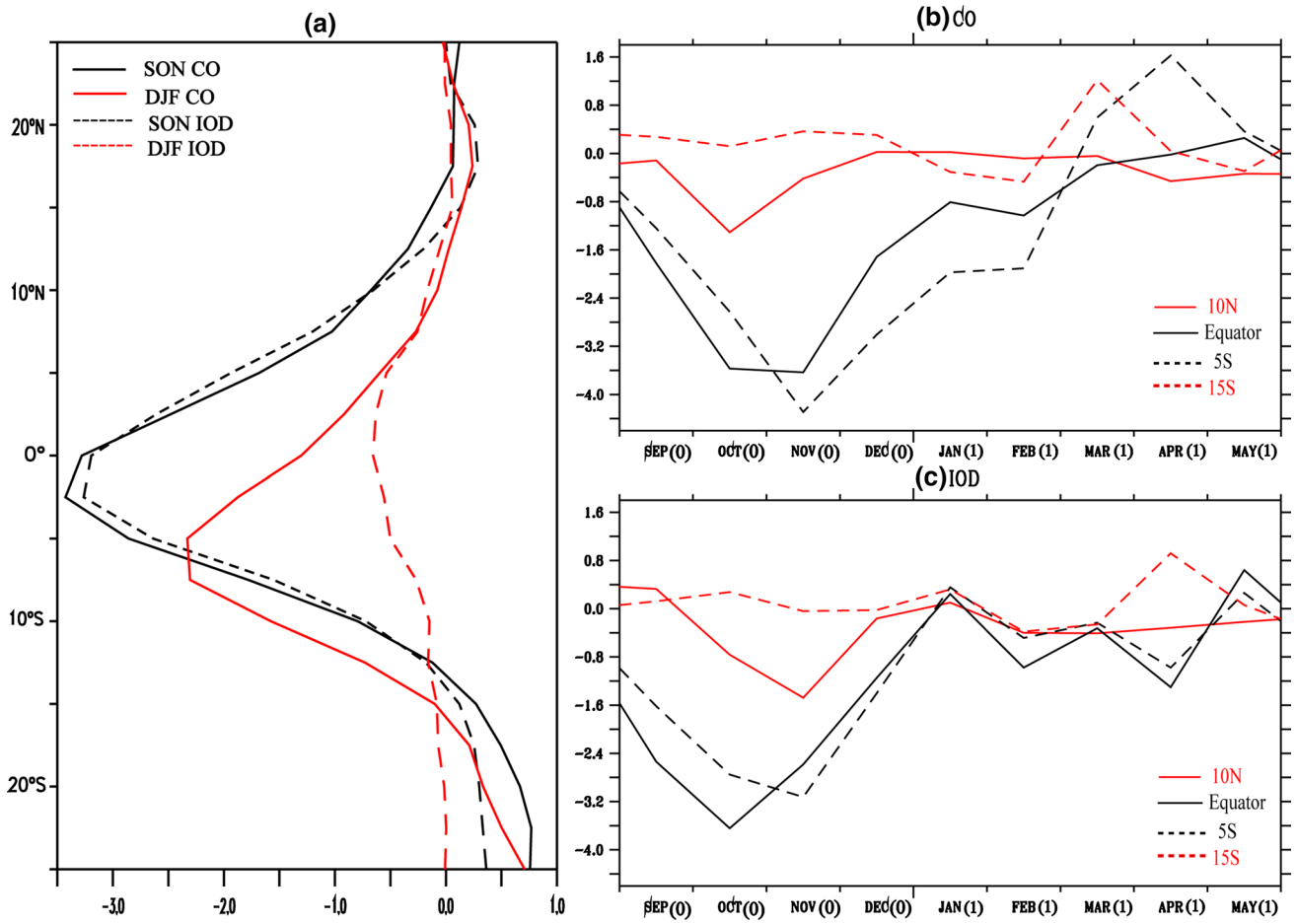

Fig. 5 **a** Latitudinal structure of zonal wind anomalies (ms^{-1}) composite during September (0)–November (0) and December (0)–February (1) for co-occurrence (*solid lines*) and pure IOD (*dashed lines*) years, temporal evolution of zonal wind anomalies (ms^{-1}) composite for **b** co-occurrence, **c** pure IOD years averaged over 70°E–100°E

co-occurrence years the IOD induced SON warming persisted up to the following spring due to the persistent El Niño forcing. It is also important to note that the warming is much stronger when local IOD forcing and remote El Niño forcing occurs simultaneously.

The leading EOF of zonal–vertical cross section (temperature) along 10°S during September to April is displayed in Fig. 7. It is important to note that this dominant pattern persists for about two seasons which indicates the possibility of an additional forcing (apart from IOD forcing) modulating this subsurface variability, as IOD forcing persists only for about a season. Previous studies (e.g. Rao et al. 2002) attributed the subsurface variability to IOD forcing. But these subsurface anomalies strengthen even after the peak IOD forcing ceases by October–November.

The above discussions strongly suggest that the variability is stronger when both TIO air–sea interaction and Pacific Ocean forcing are present. So we have considered co-occurrence, pure IOD and pure El Niño composites separately to investigate the pattern of subsurface warming. The respective composites of temperature anomalies are shown in Figs. 8, 9 and 10. In the co-occurrence composite the warming is much stronger than the other two and increases from September (0) to the following spring (Fig. 8). The warm anomalies peak in January (1) but persist up to April (1), with broader longitudinal extent than the pure IOD years. In October the maximum subsurface warm anomaly is seen at 80°E around 100 m depth whereas it is seen at 77°E at a depth of 80 m in December. It appears at 68°E in February and in April it reaches 65°E at around 60 m. It clearly reveals westward propagation of warm anomalies in the southwestern TIO. The subsurface temperature anomalies propagate along the thermocline and due to the shoaling of the mean thermocline in the western TIO and deepening of mean thermocline (and isotherms) in the east a tilted propagation towards the west is apparent. The vertical structure of temperature anomaly pattern during the co-occurrence years matches quite well with that of the first EOF.

It is important to note that the subsurface warming signals in the pure IOD composites are weaker (Fig. 9) than

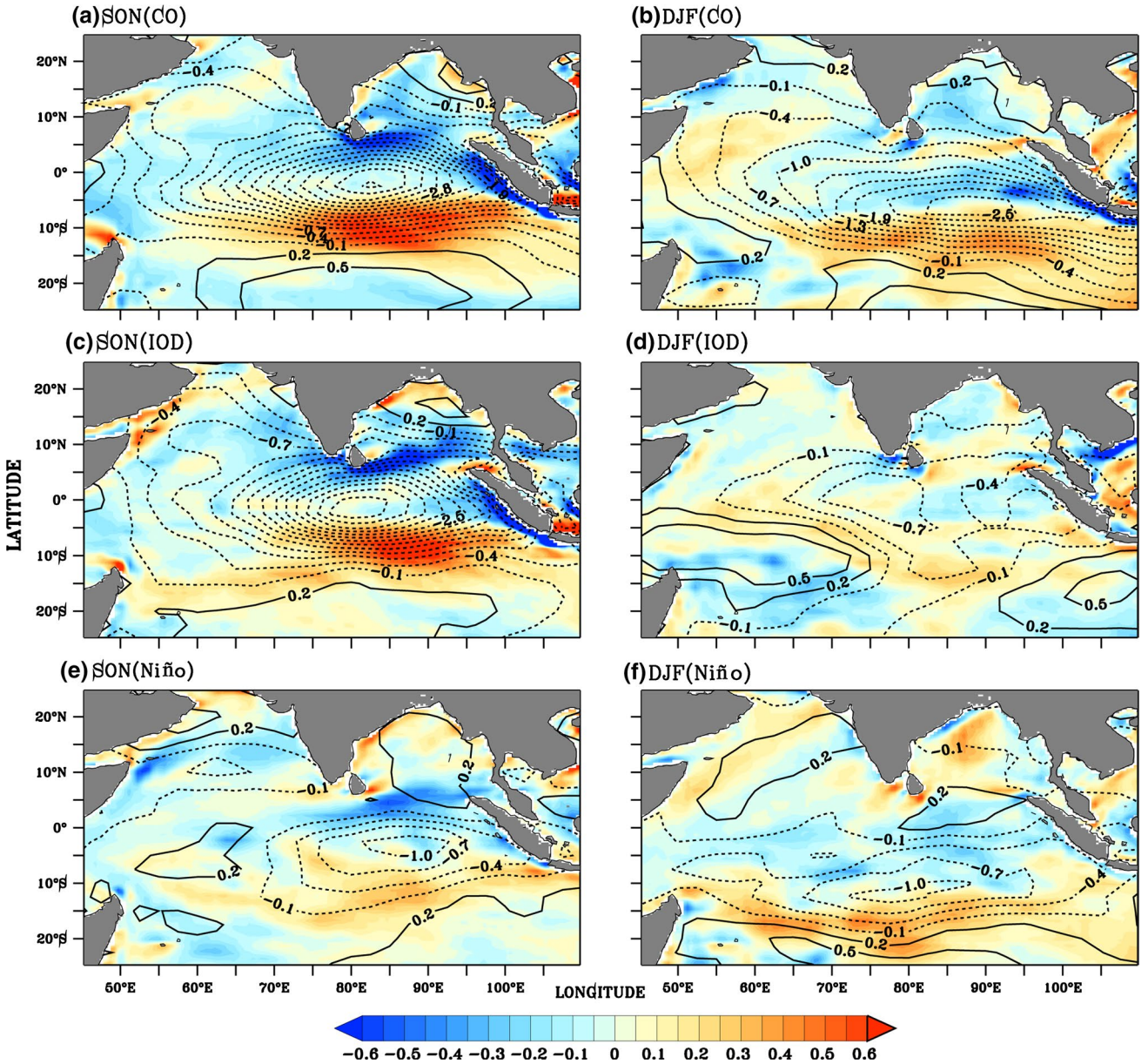

Fig. 6 Composite of anomalous wind stress curl (*shaded*, Nm^{-3}) and zonal wind (*contours*, ms^{-1}) for co-occurrence (*upper panel*) and pure IOD (*lower panel*) years for (*left panel*) September (0)–November (0) and December (0)–February (1) (*right panel*)

the co-occurrence composite. In pure IOD years the peak subsurface anomalies are evident in October–November, whereas it decays after December (Fig. 9). The westward propagation of the center of warming is not as apparent as in co-occurrence years. The warming persists for a longer period with more intensity during the co-occurrence years. This suggests the possibility of El Niño forcing modulating the TIO subsurface variability and assisting the long persistence of warming during co-occurrence years. In pure El Niño years (Fig. 10), the warm anomalies persist for a longer time and cover a broader area than the pure IOD years with an eastward extension of warming. However the pure El Niño signals are very weak in subsurface suggesting that the IOD forcing is required for the dominant subsurface variability.

It is very clear from the above discussions that the processes responsible for the subsurface temperature variability are dynamically driven. Time-longitude composite of wind stress curl anomalies are shown in Fig. 11 to demonstrate the differences in the forcing fields and their finer aspects. The strong anticyclonic wind stress curl excites downwelling Rossby wave which is evident from the SSH anomalies (contour) in all the composites (Fig. 11). Wind stress curl anomaly is stronger and extends over a broader area during the

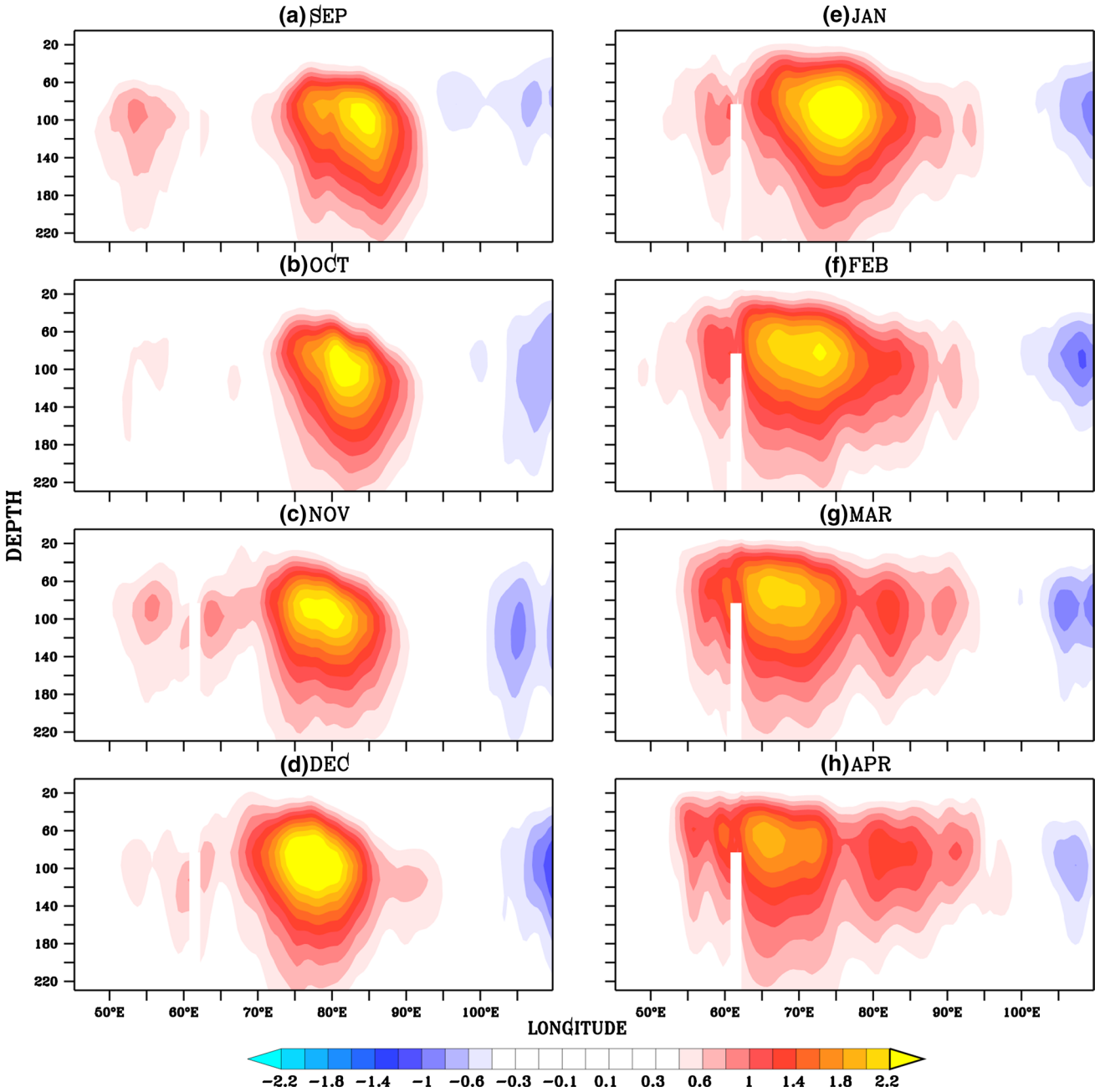

Fig. 7 Depth-longitude plot of EOF1 of temperature anomalies (°C) at 10°S during **a** September, **b** October, **c** November, **d** December, **e** January, **f** February, **g** March and **h** April

co-occurrence years compared to the pure cases and persists up to March (1) causing downwelling induced warming in the southcentral TIO (Fig. 11a). The associated Rossby wave shows westward propagation up to May (1). In IOD years cold SST anomalies in the eastern TIO induce subsidence and strong surface divergence in the east. This divergence in the east and the associated easterlies are favorable for convergence in the west inducing anomalous Indian Ocean Walker cell (Deshpande et al. 2014). These easterlies in turn can induce downwelling favorable curl (Fig. 11b). However, the anomalous wind stress curl induced by IOD forcing is seen only up to November (0). El Niño forcing also induces anomalous Walker circulation and strong subsidence in the eastern TIO. This subsidence generates anticyclonic curl anomaly which is seen in the pure El Niño composite (Fig. 11c). When both IOD and El Niño co-occur the easterlies induced by the subsidence intensify and persist for a longer time period (Fig. 6a, b). The wind stress curl induced

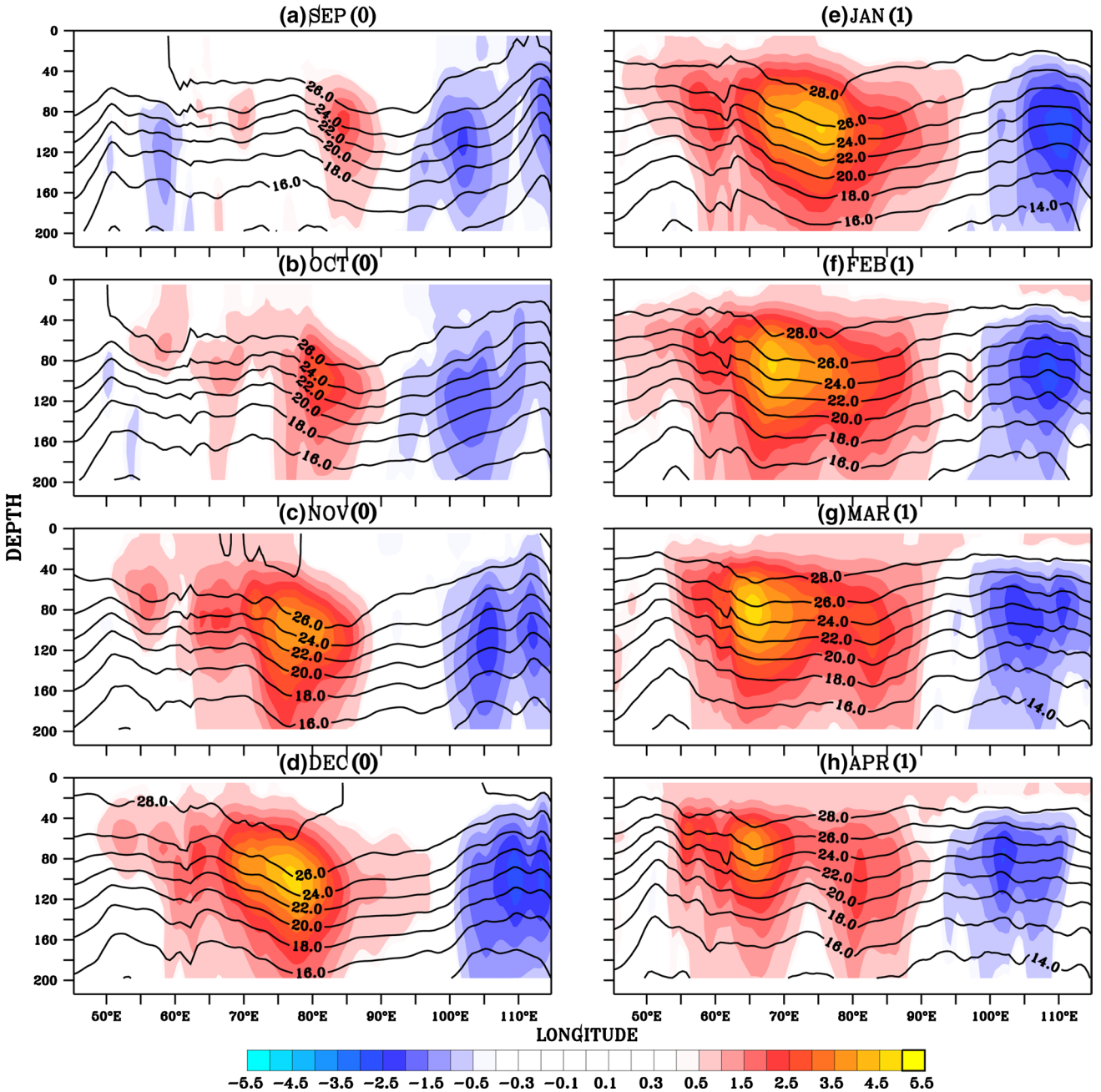

Fig. 8 Depth-longitude composite of temperature anomalies (*shaded*, °C) and mean temperature (*contours*, °C) for co-occurrence years at 10°S during **a** September (0), **b** October (0), **c** November (0), **d** December (0), **e** January (1), **f** February (1), **g** March (1) and **h** April (1)

by these easterlies strengthens downwelling in the central and western TIO. The existence of downwelling Rossby waves during El Niño and IOD years in the southern TIO is reported by several studies (Xie et al. 2002; Rao et al. 2002; Shinoda et al. 2004; Chakravorty et al. 2014). Shinoda et al. (2004) reported that the phase speed of these Rossby waves is much slower than free Rossby waves as these are continuously forced by induced Ekman convergence associated with anticyclonic surface winds. According to Xie et al. (2002) freely propagating Rossby waves behave very differently from those waves which are damped by air–sea interaction. From Fig. 11 it is clear that the phase speed of the Rossby wave is much slower than free Rossby waves in all the three composites. To examine the mechanism responsible for the persistence of the warming during the co-occurrence years, we have analyzed the BLT anomaly composite over the same region (Fig. 12). Very thick barrier layer (BL) is seen in co-occurrence years with strong westward propagation. The

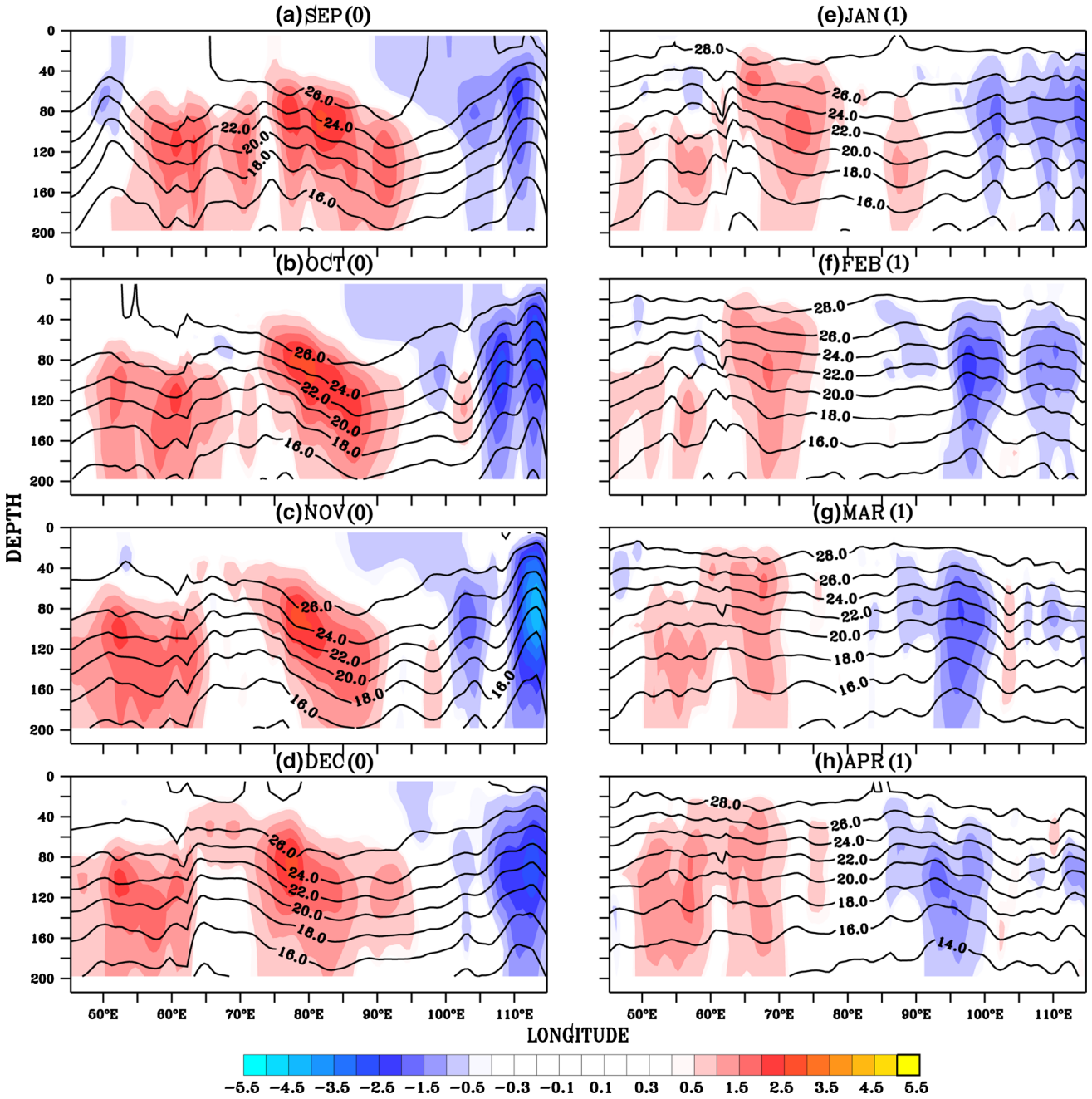

Fig. 9 Same as Fig. 8 but for pure IOD years

BL forms in the region where wind stress curl anomalies are stronger clearly indicating the role of downwelling and the associated deepening of ILD for its formation. In pure IOD and co-occurrence years negative sea surface salinity anomaly is seen in the southwestern TIO (Grunseich et al. 2011). According to Masson et al. (2004) and Thompson et al. (2006) shallow salinity stratification is seen in the equatorial Indian Ocean during the 1997–1998 co-occurrence event which favors the formation of BL. Durand et al. (2013) shows freshening of central Indian Ocean during IOD years with the recent satellite observations. All these studies support the increase of stratification in the TIO during IOD years (and co-occurrence years) which is favorable for BL formation. During co-occurrence years the BL is thickest in January (1) at 80°E and again in April (1) at 66°E where the total column water vapor (a proxy for precipitation) also shows strong anomaly. The wind stress curl and the associated downwelling help in the formation of BL and then the BL becomes thicker due to the presence of precipitation anomaly. The positive feedback between the BL and precipitation

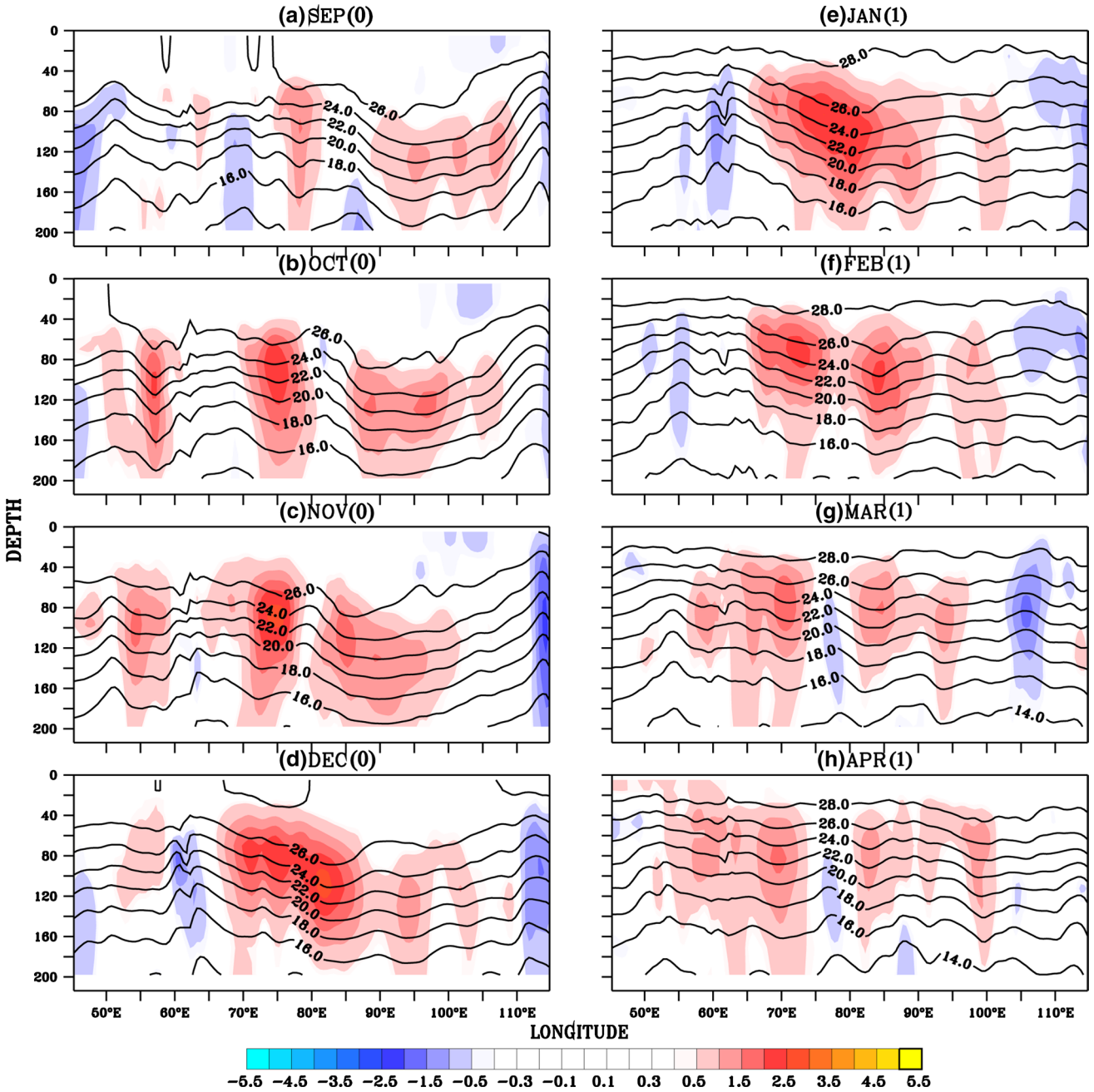

Fig. 10 Same as Fig. 8 but for pure El Niño years

through surface warming is responsible for the second peak of BL in co-occurrence years. BL persists there up to the following May (1) and enhances the surface warming by shielding the mixed layer from entering cold thermocline water. In pure IOD years strong BL forms in September but it remains almost stationary and confined to the region east of 80°E and becomes weaker after November (0). However, in pure El Niño years it persists up to February (1) but it is weaker in amplitude. The deepening of ILD due to the downwelling Rossby waves could be the possible reason for the anomalous BLT during pure El Niño years as precipitation does not support the BL formation. It is important to note that the BL is seen in the southcentral TIO during DJF where the core warming is located. This signal is very weak in pure IOD years. Thus it is very important to note that the presence of thick BL causes the subsurface warming to persist and also induces strong air–sea coupling in the southwestern TIO during the co-occurrence years.

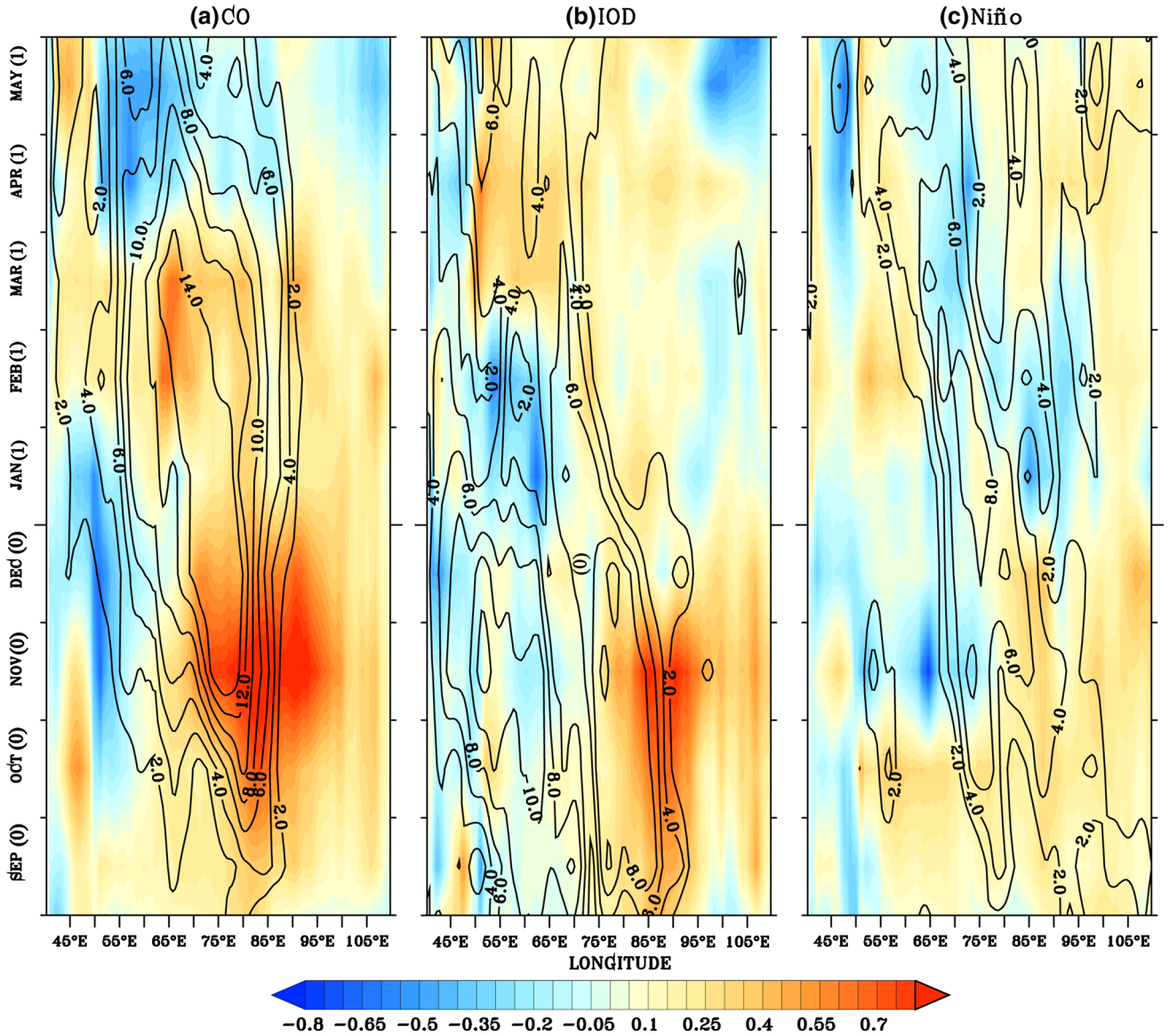

Fig. 11 Time-longitude composites of anomalous wind stress curl (*shaded*, Nm^{-3}) and SSH (*contours*, cm) for co-occurrence (*left panel*), pure IOD (*middle panel*) and pure El Niño (*right panel*) years at 10°S

4 Summary and conclusion

According to the previous studies, the dominant mode of TIO subsurface variability shows a dipole like structure and it is associated with IOD (e.g. Rao et al. 2002). However, the interannual variability of subsurface temperature and the processes responsible for this variability are not studied in detail. In this study we have shown that the leading mode of subsurface variability displays a north–south dipole pattern instead of a conventional east–west dipole. To the best of our knowledge this has not been reported before. The subsurface variability is initiated as an east–west dipole in September when IOD forcing is dominant. As the time progresses the east–west dipole weakens with the weakening IOD forcing and instead a strong north–south dipole evolves. The co-evolution of subsurface temperature with the d20 anomalies supports the role of ocean dynamics in developing such pattern of subsurface variability. We defined an index, SDI, to quantify the strength of this north–south dipole. The formation mechanism of such north–south dipole is ably supported by the meridional shear in the zonal wind anomalies which force an anticyclonic (downwelling favorable) circulation in the region south of 5°S and cyclonic (upwelling favorable) circulation north of it. In addition to that, easterly wind anomalies have a much broader meridional scale south of the equator than the north during the co-occurrence years especially from November onwards. The anomalous convection

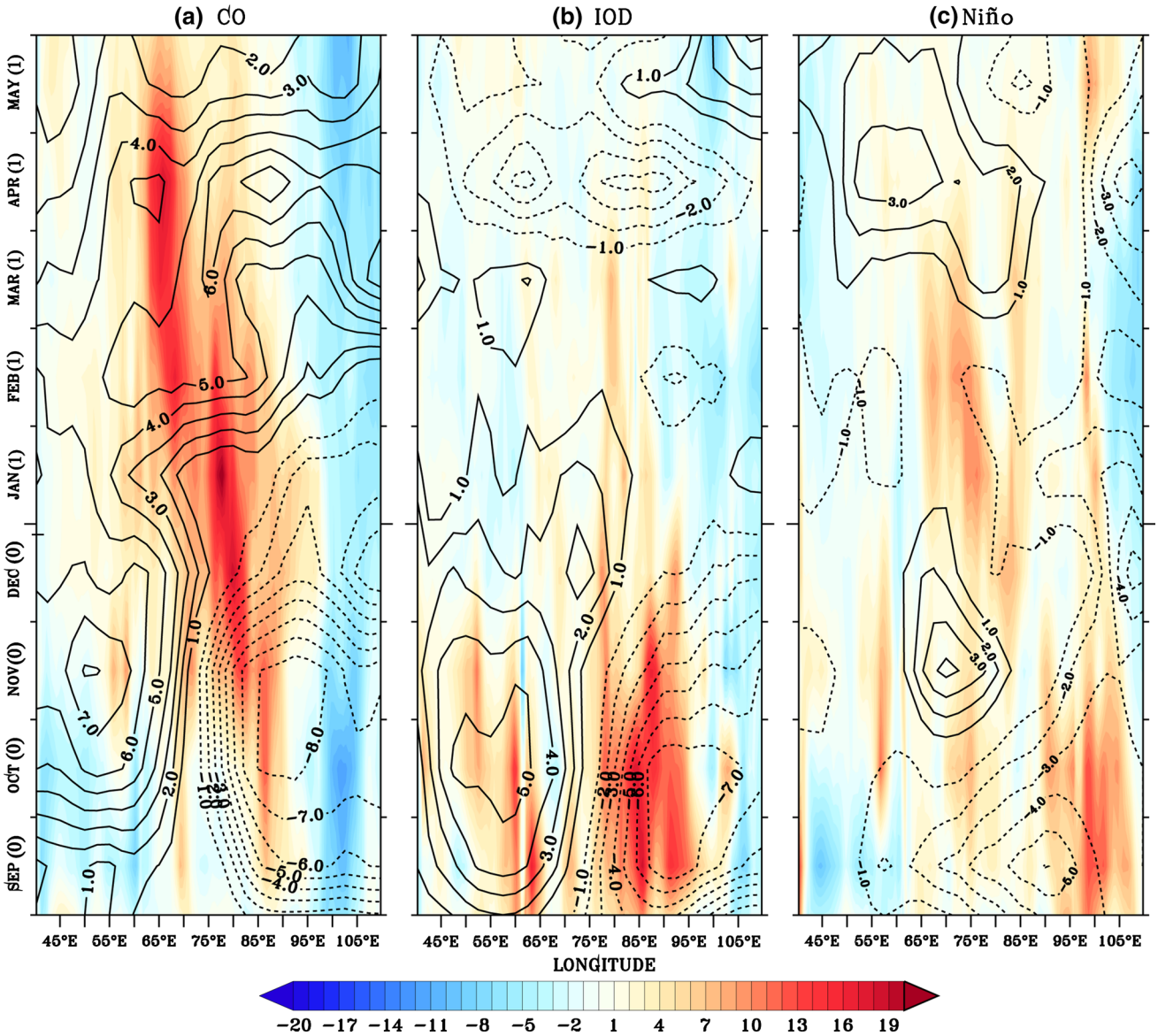

Fig. 12 Time-longitude composites of anomalous BLT (*shaded*, m) and total column water vapor (*contours*, Kg m^{-2}) for co-occurrence years (*left panel*) and pure IOD years (*middle panel*) and pure El Niño (*right panel*) at 10°S

associated with SST warming along the Rossby wave path (Xie et al. 2002) supports the persistence of easterlies with peak around 5°S favoring this subsurface dipole. These wind pattern and wind shear support positive wind stress curl anomaly in the region south of 5°S and negative anomaly in the region north of it. This anomalous wind stress curl can induce downwelling Rossby waves in south of 5°S and upwelling waves north of it (both equatorial Kelvin waves and equatorially trapped Rossby waves). Resultant upwelling Kelvin waves propagate eastward and keep the eastern TIO cool, whereas the equatorially trapped upwelling Rossby waves propagate westward. Such propagation is evident in the westward extension of cooling during the co-occurrence years. The reflected Kelvin waves from the eastern boundary and the coastal Kelvin waves further strengthen the north–south dipole. The downwelling Rossby waves in the south propagate westward and keep the western basin warm. This strongly suggests that the off-equatorial downwelling Rossby and equatorial upwelling Kelvin (Rossby) waves are inducing the north–south dipole pattern in subsurface temperature variability. It is important to highlight that IOD years are characterized by a conventional east–west dipole pattern whereas co-occurrence years are characterized by a north–south dipole pattern with cold anomalies in the north (70°E–100°E, 5°S–10°N) and warm anomalies in the south (60°E–90°E, 15°S–5°S).

Such a north–south pattern is not visible in the surface as the cooling induced by the upwelling waves are overcome by the surface heat flux (dominated by the clear sky short wave radiation associated with the subsidence) induced warming. This further suggests the role of ocean dynamics in maintaining such north–south dipole pattern over three seasons.

The variability is more apparent when we examined the EOF of d20 and 100 m temperature anomaly for three seasons (SON, DJF and MAM) separately. In SON the first mode of variability is associated with IOD. But in DJF the leading mode of variability corresponds to co-occurrence years. The most interesting point is that the subsurface temperature shows significant variability in MAM also and the PC corresponds only to co-occurrence years. The seasonal composite of d20 and 100 m temperature anomaly in co-occurrence and pure IOD years also support this hypothesis. It is important to note that the subsurface variability in the TIO during spring season is not explored in any previous studies. The north–south dipole pattern is much clear in the co-occurrence composite which strengthens in DJF and persists up to MAM. On the other hand in pure IOD years, the anomalies are much weaker with an east–west dipole pattern and are limited to SON.

The vertical structure of western warming displays the characteristic features of Rossby waves in the southwestern TIO. In co-occurrence years a strong central TIO warming is seen from September onwards with characteristics of slow westward propagation persisting up to the following April. But in pure IOD years this warming is much weaker and it doesn't persist for such a long time period. The westward propagation of subsurface warming in co-occurrence years account for the possible thermocline SST interaction in the southwestern TIO as in Xie et al. (2002) and Chowdary et al. (2009). The downwelling favorable wind stress curl anomalies force anomalous subsurface warming. In co-occurrence years the wind stress curl anomaly is much stronger and as a result stronger Rossby wave is generated which then propagates to the western TIO by April (1). But in pure IOD case the wave propagation is weaker and stays for a shorter time. The anomalous south-easterly winds which form during IOD and the subsidence caused by El Niño together generate a stronger downwelling in co-occurrence years than the pure cases where the feedback mechanism is weak. In IOD years the western TIO is warmer and thus convection forms over that region. This induces convergence of winds and as a result the anomalous easterly winds are shifted towards central TIO. But they do not persist for a longer time as the feedback mechanism is weak. In El Niño years the zonal sea level pressure gradient supports the anomalous circulation.

The SST warming along the Rossby wave path induces excess precipitation (Xie et al. 2002) and the resultant fresh water flux increases upper ocean stratification and the possibility of barrier layer formation. The long persistence of the warming can be explained by the formation of BL which inhibits entrainment cooling and turbulent mixing and thus helps to sustain the warming. In the co-occurrence years the westward propagation of BLT anomaly is similar to the warming which indicates the role of BL in the persistence of warming in the western TIO. The composite of total column water vapor anomaly supports strong air–sea interaction in co-occurrence years. It is found that TIO forcing is responsible for the generation of strong subsurface variability whereas both TIO and Pacific forcing are required for its persistence. The southwestern TIO emerges as a climatically important region (Schott et al. 2009) where the Madden Julian Oscillation (MJO) forms and propagates eastward due to very shallow mean thermocline (Wheeler and Hendon 2004; Zhang 2005; Jayakumar et al. 2011) favoring strong air–sea interaction. Any subsurface variability over this region during winter/spring season is very crucial for MJO activities.

Acknowledgments Sayantani acknowledges Council of Scientific and Industrial Research (CSIR), India for research fellowship. Authors acknowledge Director, IITM for support and encouragement. The valuable suggestions and comments from the anonymous reviewers helped us to improve the manuscript considerably.

References

Alexander MA, Bladé I, Newman M, Lanzante JR, Lau N-C, Scott JD (2002) The atmospheric bridge: the influence of ENSO teleconnections on air–sea interaction over the global oceans. J Clim 15:2205–2231

Annamalai H, Murtugudde R, Potemra J, Xie S-P, Liu P, Wang B (2003) Coupled dynamics over the Indian Ocean: spring initiation of the zonal mode. Deep Sea Res Part 2 50:2305–2330

Behera SK, Luo J-J, Masson S, Rao SA, Sakuma H, Yamagata T (2006) A CGCM study on the interaction between IOD and ENSO. J Clim 19:1688–1705

Bjerknes J (1969) Atmospheric teleconnections from the equatorial Pacific. Mon Weather Rev 97:163–172

Carton JA, Giese BS (2008) A reanalysis of ocean climate using Simple Ocean Data Assimilation (SODA). Mon Weather Rev 136:2999–3017

Chakravorty S, Gnanaseelan C, Chowdary JS, Luo J-J (2014) Relative role of El Niño and IOD forcing on the southern tropical Indian Ocean Rossby waves. J Geophys Res 1–18. doi:10.1002/2013JC009713

Chambers DP, Tapley BD, Stewart RH (1999) Anomalous warming in the Indian Ocean coincident with El Niño. J Geophys Res 104:3035–3047

Chowdary JS, Gnanaseelan C (2007) Basin wide warming of the Indian Ocean during El Niño and Indian Ocean dipole years. Int J Climatol 27:1421–1438. doi:10.1002/joc.1482

Chowdary JS, Gnanaseelan C, Xie S-P (2009) Westward propagation of barrier layer formation in the 2006–2007 Rossby wave events over the tropical southwest Indian Ocean. Geophys Res Lett 36:L04607. doi:10.1029/2008GL036642

Deshpande A, Chowdary JS, Gnanaseelan C (2014) Role of thermocline–SST coupling in the evolution of IOD events and their regional impacts. Clim Dyn 1–12. doi:10.1007/s00382-013-1879-5

Durand F, Alory G, Dussin R, Reul N (2013) SMOS reveals the signature of Indian Ocean Dipole events. Ocean Dyn 63:1203–1212

Gnanaseelan C, Vaid BH (2010) Interannual variability in the biannual Rossby waves in the tropical Indian Ocean and its relation to Indian Ocean dipole and El Niño forcing. Ocean Dyn 60(1):27–40

Gnanaseelan C, Vaid BH, Polito PS (2008) Impact of biannual Rossby waves on the Indian Ocean Dipole. IEEE Geosci Remote Sens Lett. doi:10.1109/LGRS.2008.919505

Gnanaseelan C, Deshpande A, McPhaden MJ (2012) Impact of Indian Ocean Dipole and El Niño/Southern Oscillation wind-forcing on the Wyrtki jets. J Geophys Res 117:C08005. doi:10.1029/2012JC007918

Grunseich G, Subrahmanyam B, Murty VSN, Giese BS (2011) Sea surface salinity variability during the Indian Ocean Dipole and ENSO events in the tropical Indian Ocean. J Geophys Res 116:C11013. doi:10.1029/2011JC007456

Huang B, Kinter JL III (2002) Interannual variability in the tropical Indian Ocean. J Geophys Res 107(C11):3199. doi:10.1029/2001JC001278

Jayakumar A, Vialard J, Lengaigne M, Gnanaseelan C, McCreary JP, Praveen Kumar B (2011) Processes controlling the surface temperature signature of the Madden–Julian oscillation in the thermocline ridge of the Indian Ocean. Clim Dyn 37:2217–2234

Kara AB, Rochford PA, Hulburt HE (2000) Mixed layer depth variability and barrier layer formation over the North Pacific Ocean. J Geophys Res 105:16803–16821

Klein SA, Soden BJ, Lau NC (1999) Remote sea surface temperature variations during ENSO: evidence for a tropical atmospheric bridge. J Clim 12:917–932

Lau NC, Nath MJ (2000) Impact of ENSO on the variability of the Asian–Australian monsoon as simulated in GCM experiments. J Clim 13:4287–4309

Lukas R, Lindstorm E (1991) The mixed layer of the western equatorial Pacific Ocean. J Geophys Res 96:3343–3357

Masson S, Boulanger JP, Menkes C, Delecluse P, Yamagata T (2004) Impact of salinity on the 1997 Indian Ocean Dipole event in a numerical experiment. J Geophys Res 109:C02002. doi:10.1029/2003JC001807

Meyers G, McIntosh P, Pigot L, Pook M (2007) The years of El Niño, La Niña, and interactions with the tropical Indian Ocean. J Clim 20:2872–2880. doi:10.1175/JCLI4152.1

Murtugudde R, McCreary JP, Busalacchi AJ (2000) Oceanic processe associated with anomalous events in the Indian Ocean with relevance to 1997–1998. J Geophys Res 105(C2):3295–3306. doi:10.1029/1999JC900294

Neelin JD, Battisti SD, Hirst AC, Jin FF, Wakata Y, Yamagata T, Zebiak E (1998) ENSO theory. J Geophys Res 103:14261–14290

Nigam S, Shen HS (1993) Structure of oceanic and atmospheric low-frequency variability over the tropical Pacific and Indian Oceans. Part I: COADS observations. J Clim 6:657–676

Rao SA, Behera SK (2005) Subsurface influence on SST in the tropical Indian Ocean: structure and interannual variability. Dyn Atmos Oceans 39:103–135

Rao SA, Behera SK, Masumoto Y, Yamagata T (2002) Interannual subsurface variability in the tropical Indian Ocean with a special emphasis on the Indian Ocean dipole. Deep Sea Res II 49:1549–1572

Rao RR, Kumar G, Ravichandran M, Rao AR, Gopalakrishna VV, Thadathil P (2010) Interannual variability of Kelvin wave propagation in the wave guides of the equatorial Indian Ocean, the coastal Bay of Bengal and the southeastern Arabian Sea during 1993–2006. Deep Sea Res Part I 57:1–13

Saji NH, Yamagata T (2003) Possible impacts of Indian Ocean dipole mode events on global climate. Clim Res 25:151–169. doi:10.3354/cr025151

Saji NH, Goswami BN, Vinayachandran PN, Yamagata T (1999) A dipole mode in the tropical Indian Ocean. Nature 401:360–363. doi:10.1038/43854

Sayantani O, Gnanaseelan C, Chowdary JS (2013) The role of Arabian Sea in the evolution of Indian Ocean Dipole. Int J Climatol. doi:10.1002/joc.3805

Schott FA, Xie S-P, McCreary JP (2009) Indian Ocean circulation and climate variability. Rev Geophys 47:RG1002. doi:10.1029/2007RG000245

Shinoda T, Hendon HH, Alexander MA (2004) Surface and subsurface dipole variability in the Indian Ocean and its relation to ENSO. Deep Sea Res Part I Oceanogr Res Pap 51(619):635. doi:10.1016/j.dsr.2004.01.005

Simmons AJ, Gibson JK (2000) The ERA-40 project plan, ERA-40 project report series, 1. ECMWF, Shinfield Park, Reading, p 63

Sprintall J, Tomczak M (1992) Evidence of barrier layer in the surface layer of the tropics. J Geophys Res 97:7305–7316

Sreenivas P, Gnanaseelan C, Prasad K (2012) Influence of El Niño and Indian Ocean Dipole on sea level variability in the Bay of Bengal. Global Planet Change 80:215–225

Thompson B, Gnanaseelan C, Salvekar PS (2006) Variability in the Indian Ocean circulation and salinity and its impact on SST anomalies during dipole events. J Mar Res 64:853–880

Uppala SM et al (2005) The ERA-40 re-analysis. Q J R Meteorol Soc 131:2961–3012. doi:10.1256/qj.04.176

Webster PJ, Moore AW, Loschnigg JP, Leben RR (1999) Coupled ocean atmosphere dynamics in the Indian Ocean during 1997–1998. Nature 401:356–360. doi:10.1038/43848

Wheeler MC, Hendon HH (2004) An all-season real-time multivariate MJO index: development of an index for monitoring and prediction. Mon Weather Rev 132:1917–1932

Xie S-P, Annamalai H, Schott F, McCreary JP (2002) Structure and mechanisms of south Indian Ocean climate variability. J Clim 15:864–878

Yang J, Liu Q, Xie S-P, Liu Z, Wu L (2007) Impact of the Indian Ocean SST basin mode on the Asian summer monsoon. Geophys Res Lett 34:L02708. doi:10.1029/2006GL028571

Yu L, Reinecker MM (1999) Mechanism of the Indian Ocean warming during 1997–1998 El Niño. Geophys Res Lett 26:735–738

Yu W, Xiang B, Liu L, Liu N (2005) Understanding the origins of interannual thermocline variations in the tropical Indian Ocean. Geophys Res Lett 32:L24706. doi:10.1029/2005GL024327

Zhang C (2005) The Madden–Julian oscillation. Rev Geophys 43:2003. doi:10.1029/2004RG000158